ACS APPLIED MATERIALS & INTERFACES

Research Article

www.acsami.org

Investigation of Solution-Processed Ultrathin Electron Injection Layers for Organic Light-Emitting Diodes

Sebastian Stolz,*[,†,‡] Michael Scherer,[‡,§] Eric Mankel,[‡,⊥] Robert Lovrinčić,[‡,§] Janusz Schinke,[‡,§] Wolfgang Kowalsky,[‡,§] Wolfram Jaegermann,[⊥] Uli Lemmer,[†,#] Norman Mechau,[†,‡] and Gerardo Hernandez-Sosa[†,‡,#]

[†]Light Technology Institute, Karlsruhe Institute of Technology, Engesserstrasse 13, 76131 Karlsruhe, Germany

[‡]InnovationLab GmbH, Speyerer Strasse 4, 69115 Heidelberg, Germany

[§]Institut für Hochfrequenztechnik, Technische Universität Braunschweig, Schleinitzstrasse 22, 38106 Braunschweig, Germany

[⊥]Surface Science Division, Materials Science Institute, Technische Universität Darmstadt, Jovanka-Bontschits-Strasse 2, 64287 Darmstadt, Germany

[#]Institute of Microstructure Technology, Karlsruhe Institute of Technology, Hermann-von-Helmholtz-Platz 1, 76344 Eggenstein-Leopoldshafen, Germany

Supporting Information

ABSTRACT: We study two types of water/alcohol-soluble aliphatic amines, polyethylenimine (PEI) and polyethylenimine-ethoxylated (PEIE), for their suitability as electron injection layers in solution-processed blue fluorescent organic light-emitting diodes (OLEDs). X-ray photoelectron spectroscopy is used to determine the nominal thickness of the polymer layers while ultraviolet photoelectron spectroscopy is carried out to determine the induced work-function change of the silver cathode. The determined work-function shifts are as high as 1.5 eV for PEI and 1.3 eV for PEIE. Furthermore, atomic force microscopy images reveal that homogeneous PEI and PEIE layers are present at nominal thicknesses of about 11 nm. Finally, we solution prepare blue emitting polymer-based OLEDs using PEI/PEIE in combination with Ag as cathode layers. Luminous efficiency reaches 3 and 2.2 cd A^{-1}, whereas maximum luminance values are as high as 8000 and 3000 cd m^{-2} for PEI and PEIE injection layers, respectively. The prepared devices show a comparable performance to Ca/Ag OLEDs and an improved shelf lifetime.

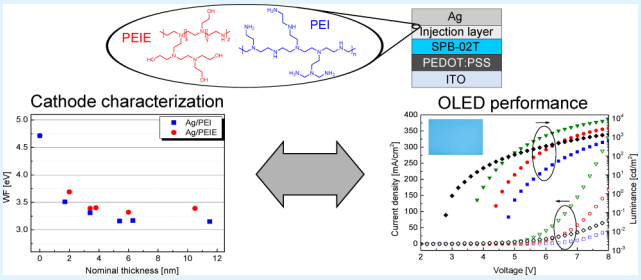

KEYWORDS: *polyethylenimine, polyethylenimine-ethoxylated, injection layers, photoelectron spectroscopy, OLEDs, printed electronics*

INTRODUCTION

Large-area solid-state lighting and TFT displays based on fully printed organic light-emitting diodes (OLEDs) require the development of stable and efficient solution-processable cathode materials. One obstacle for the production of OLEDs by high throughput printing techniques is the current use of either alkali salts or low-work-function alkaline earth metals like calcium or barium as cathode materials. These materials are highly reactive, and thus they cannot be easily solution-processed but have to be evaporated. Furthermore, humidity oxidizes these cathode layers, limiting the lifetime of OLEDs.[1−5] In addition, it has been shown that already submonolayers of Ca and Ba quench the photoluminance of organic emitter materials.[6−9]

One promising approach for solution processable cathode layers is the use of air-stable metals like aluminum or silver in combination with water/alcohol-soluble electron injection layers. Its solubility in highly polar solvents enables these materials to be used in multilayer device architectures, as commonly used emitting materials for OLEDs are not soluble in highly polar solvents. In this context, different salts as well as organic polymers with polar side chains have attracted attention over the course of the last few years. Solution-processed cesium carbonate and cesium stearate have been shown to be an efficient electron injection layer for OLEDs if used in combination with Al.[10−13] However, Al cannot be solution-processed but needs to be evaporated.

Several research groups have demonstrated that conjugated polymers can be effectively used as electron injection layers in OLEDs. In this respect, amino- or ammonium-conjugated polymers have received a lot of attention during the last few years.[14−19] Amino-conjugated polymers usually require the addition of small amounts of acetic acid to dissolve them in polar solvents. To remove the acetic acid, these materials need

Received: January 14, 2014
Accepted: April 4, 2014
Published: April 4, 2014

   dx.doi.org/10.1021/am500287y | ACS Appl. Mater. Interfaces 2014, 6, 6616−6622

to be dried in vacuum, making the OLED preparation more laborious.[20] In contrast, ammonium-conjugated polymers are instrinsically soluble in highly polar solvents, but usually suffer from ion migration because of their cationic nature. This can negatively affect the turn-on times of OLEDs.[14,15] Therefore, nonionic water/alcohol-soluble polymers, which can be used as electron injection materials, are more desirable.

Aliphatic amines, such as polyethylenimine (PEI) and polyethylenimine-ethoxylated (PEIE), fulfill these requirements. It was demonstrated that 10 nm of PEI and PEIE lower the work function of a variety of conducting substrates through the formation of interface dipoles by about 1 eV.[21−23] In 2008, Xiong et al. demonstrated efficient bottom-emissive evaporated OLEDs using PEIE in combination with ITO as cathode layer.[24] Zhou et al. built efficient OLEDs with PEIE-coated aluminum as cathode material, where all functional layers besides PEIE were evaporated.[21] Recently, Kim et al. prepared highly efficient inverted OLEDs by using PEI and ZnO as cathode material.[25] However, only PEI and the emitting layer were solution-processed. Furthermore, it was recently shown that annealed PEI and PEIE (PEI(E)) layers are insoluble in organic solvents.[26] This could offer the possibility of fully solution processed OLEDs by using PEI(E) in combination with a printed metal electrode.

In this work, we present efficient solution-processed blue fluorescent OLEDs using PEI(E) as electron injection layer and investigate the correlation between OLED performance and cathode properties. In contrast to previous work by other research groups, three out of four functional layers are solution processed with only the Ag cathode contact being evaporated. As Ag can be printed by various printing techniques, the used stack is very close to real world printing applications.[27−30] In the first instance, we examine the influence of the PEI(E) thickness on the WF of evaporated Ag layers. X-ray photoelectron spectroscopy (XPS) is used to estimate the thickness of the prepared polymer layers and values between 2 and 12 nm are found. The resulting work-function shifts of the Ag substrates are measured by Ultraviolet photoelectron spectroscopy (UPS). These are as high as 1.5 eV for PEI and 1.3 eV for PEIE. Furthermore, the determined work functions show a strong thickness dependency for small PEI(E) thicknesses and a saturation for larger thicknesses. AFM images indicate that the existence of these two regimes is related to the polymer coverage of the Ag surface. In the case of small thicknesses, the Ag surface is only partially covered, whereas it is fully covered for larger thicknesses.

Subsequently, we solution-prepare blue fluorescent OLEDs and vary the nominal thickness of the PEI(E) layers. Optimal PEI and PEIE thicknesses yield a maximum luminance of about 4× and 1.5× the maximum value observed for our Ca reference OLEDs. Finally, we show that OLEDs using PEI(E) as electron injection layer exhibit improved shelf lifetimes compared to Ca-OLEDs.

RESULTS AND DISCUSSIONS

Characterization of PEI(E) Films on top of Ag. To produce PEI(E) layers with different thicknesses, we dissolved both polymers in 2-methoxyethanol with various concentrations and spin-coated the solutions on top of silver samples. X-ray photoelectron spectroscopy (XPS) was used to measure the thickness of the polymer layers as it was too low to be reliably measured by a profilometer. Panels a and b in Figure 1 show XPS measurements of the silver 3d signal of the PEI and

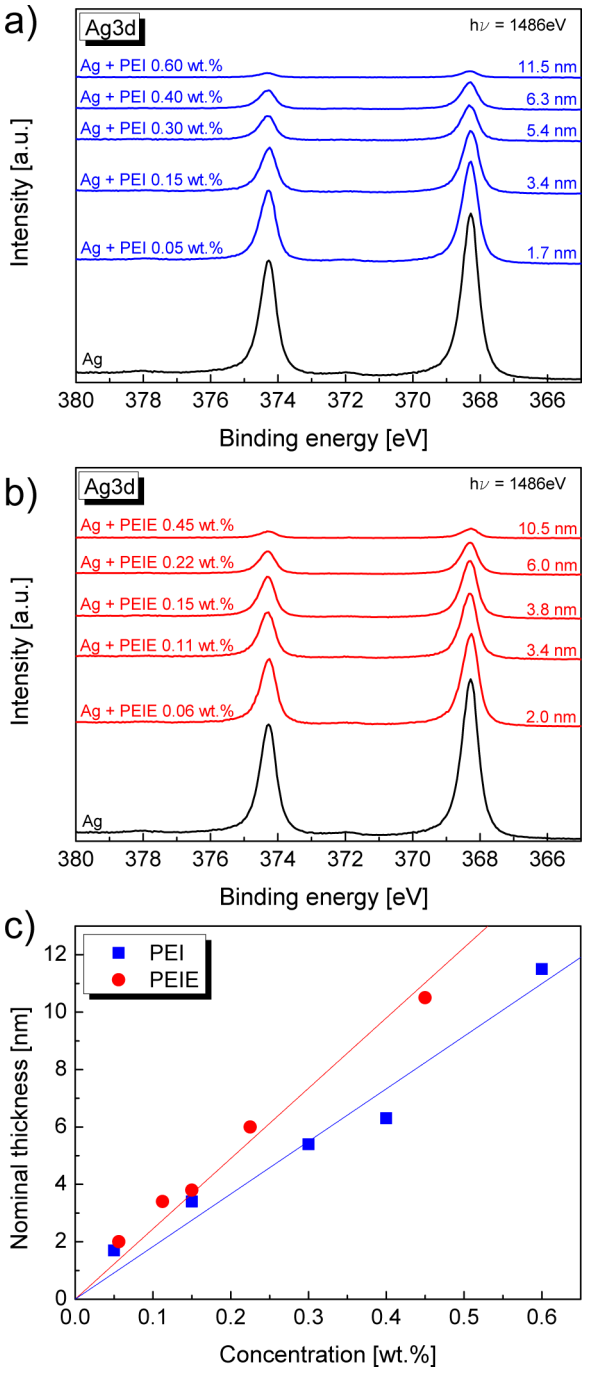

Figure 1. XP-spectra of silver samples with spin-coated layers of (a) PEI and (b) PEIE on top. (c) Nominal thickness of PEI and PEIE plotted against the concentration of spin-coated solutions. The determined thickness values follow a linear relation with respect to the polymer concentration.

PEIE samples, respectively. As it can be seen, the 3d peak of the silver layer is damped by the overlying polymer layer. This can be used to estimate the nominal thickness of the PEI(E) layers as

$$d = \lambda \ln\left(\frac{I_0}{I}\right) \tag{1}$$

under the assumption that a closed polymer layer is present.[31] Here, I and I_0 are the integrated intensities of the Ag 3d signals of the Ag/PEI(E) and pure Ag samples, respectively. The

dx.doi.org/10.1021/am500287y | ACS Appl. Mater. Interfaces 2014, 6, 6616−6622

inelastic mean free path of the Ag 3d photoelectrons within the PEI(E) layer, λ, can be calculated according to the formula by Gries.[32]

Measured nominal thicknesses increase for both PEI and PEIE with increasing polymer concentration at constant spin-coating parameters. In the case of PEI, the determined values are between 3.4 nm for a concentration of 0.15 wt % and 11.5 nm for a concentration of 0.6 wt %. For PEIE, nominal thicknesses are between 2 nm for a concentration of 0.06 wt % and 10.5 nm for a concentration of 0.45 wt %. In Figure 1c, the determined nominal thicknesses are plotted against the corresponding concentration. It can be seen that the determined values follow a linear relation with respect to the polymer concentration.

The same samples were characterized by ultraviolet photoelectron spectroscopy (UPS) in order to determine their work function Φ (Figure 2, the corresponding secondary electron edge spectra can be seen in Figure S1 in the Supporting Information). For a 1.7 nm thick layer of PEI we measure a decrease of the work function of silver by $\Delta\Phi$ = 1.15 eV from about 4.65 eV to a value of about 3.5 eV. Increasing the PEI thickness to 3.4 and 5.4 nm leads to an even larger reduction of the work function by about $\Delta\Phi$ = 1.35 eV and $\Delta\Phi$ = 1.5 eV to values of 3.3 and 3.15 eV. At this thickness, the work function saturates and a further increase in nominal polymer thickness to 6.3 and 11.5 nm does not lead to a further reduction of the work function. In the case of PEIE, the same behavior was observed. Whereas for a nominal thickness of 2 nm a reduction of the work function by $\Delta\Phi$ = 1 eV was determined, a PEIE layer of 3.4 nm reduced the work function by $\Delta\Phi$ = 1.25 eV to a value of about 3.4 eV. At this point, the work function starts to saturate and a further increase in nominal polymer thickness up to a maximal value of 10.5 nm leads just to a marginal decrease with a minimal value of about 3.35 eV.

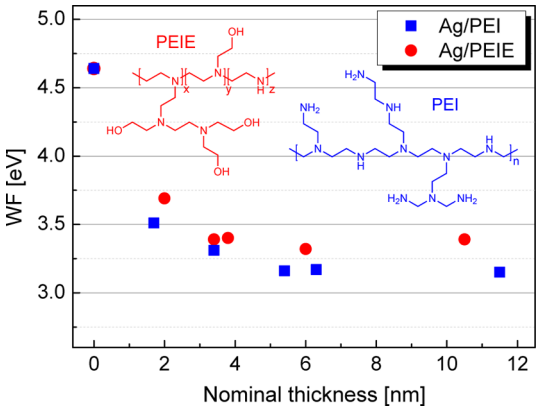

Figure 2. Work function of silver samples covered with PEI/PEIE layers of different thicknesses measured by UPS. Polymer layer thicknesses were estimated by XPS (see Figure 1).

The work-function reduction induced by PEI(E) has been attributed to the formation of interface dipoles because of the polymers' polar side chains (see inset of Figure 2) and a charge transfer between substrate and PEI(E).[21] However, the exact working mechanism is still the subject of ongoing research. Kang et al. recently proposed a process of electrostatic self-assembly between protonated PEI(E) amine groups and ITO oxygen atoms to explain the WF reduction induced by PEI(E).[33] However, this process relies on the existence of oxygen on the substrate surface. In our work, PEI(E) was applied onto a clean Ag surface, with only a small amount of adsorbed oxygen present at the surface (see Figure S2 in the Supporting Information). Moreover, XP-spectra of our PEI(E) layers on Ag show a symmetric N 1s core level (see Figure S3 in the Supporting Information). This indicates that all nitrogen atoms have the same oxidation state and thus no protonated amine groups are present in our samples. These findings suggest that the WF reduction of Ag cannot be explained by the mechanism proposed by Kang et al.

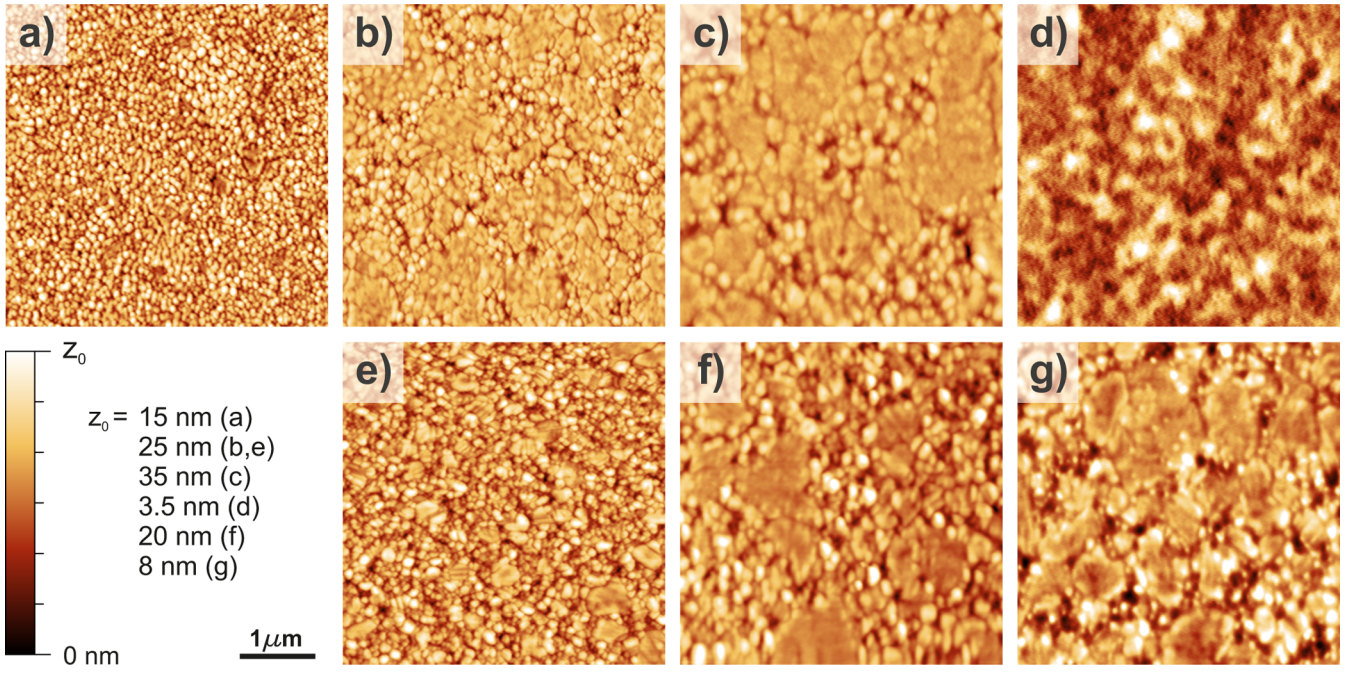

Figure 3. AFM images of (a) Ag, Ag/PEI with nominal polymer thicknesses of (b) 1.7, (c) 3.4, and (d) 11.5 nm and Ag/PEIE with nominal polymer thicknesses of (e) 2.0, (f) 3.8, and (g) 10.5 nm.

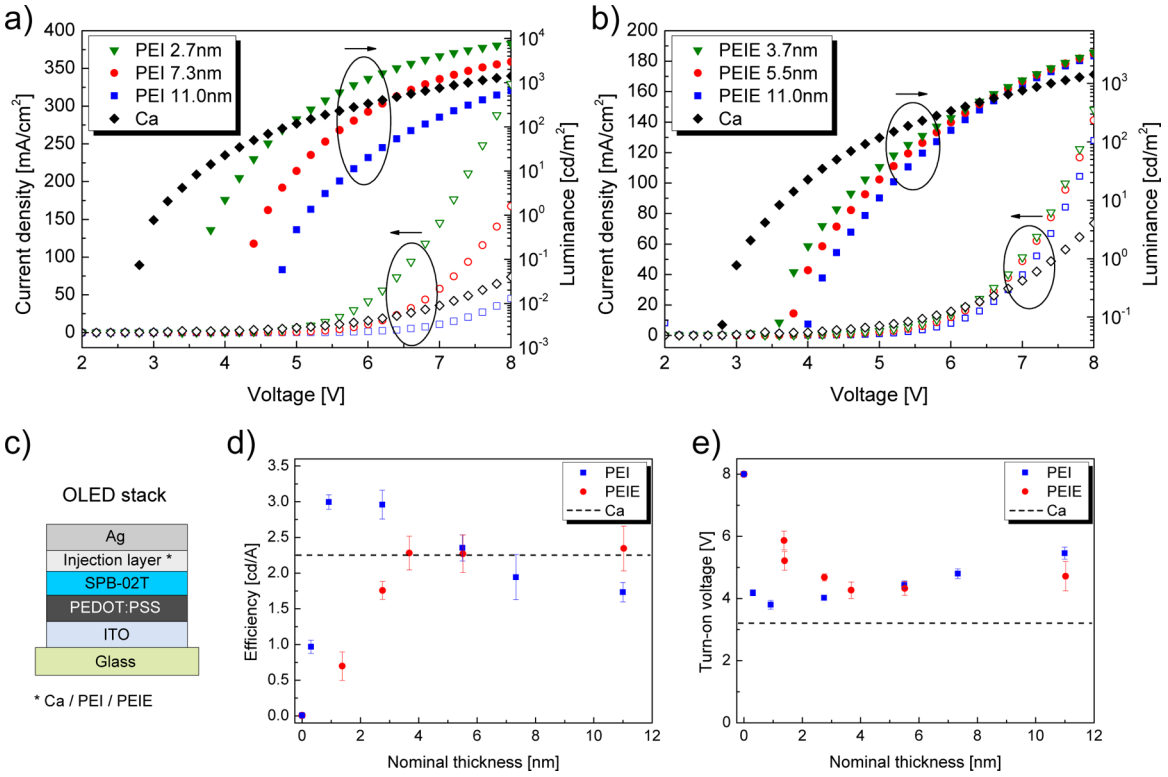

Figure 4. (a, b) LIV characteristics of the prepared OLEDs. (c) OLED stack. (d, e) Luminous efficiency and turn-on voltage of the OLEDs. For each data point, at least four devices were prepared and averaged.

The thickness dependency of the work function at lower nominal thicknesses and saturation at larger nominal thicknesses can be explained by the surface coverage of the samples. Figure 3 shows AFM topography images of Ag and Ag/PEI(E) samples with different nominal polymer thicknesses. In Figure 3a, the grain like topography of a pure silver sample is presented. When a 0.9 nm thick PEI layer is spin-coated on top (Figure 3b), flake or island like structures with a size of about 1 μm develop. As the PEI thickness is increased to 2.7 nm (Figure 3c), these structures are growing and the underlying silver features are not visible anymore. Finally, Figure 3d shows the topography of an Ag/PEI sample with a nominal thickness of 11 nm. Here, the topography is very smooth with a roughness (root-mean-square) of <1 nm compared to values between 2.5 and 3.2 nm for the other three samples, suggesting that a homogeneous PEI layer has formed. In case of PEIE, the situation is very similar (Figures 3e–g). With increasing nominal polymer thickness, surface coverage of the underlying silver layer is increasing until a homogeneous PEIE layer is present at a nominal thickness of 12.2 nm.

The AFM findings are in good agreement with the observed work functions in Figure 2. As it was published elsewhere, the reduction of the Ag work function is due to an interaction between the metal and the polymer.[21] Thus, the maximum shift in work function is expected when the polymer layer on top of silver is closed as a further increase in nominal thickness does not have any influence on the metal/polymer contact area anymore. A PEI layer with a nominal thickness of 2.7 nm covers the underlying silver layer almost completely. Therefore, the work function starts to saturate at this thickness (Figure 2). In the case of PEIE, the saturation regime of the measured work functions starts between 4 and 6 nm. Consequently, the underlying silver layer is mostly covered at this thickness (Figure 3f).

Performance of PEI(E) OLEDs. To evaluate the suitability of PEI and PEIE as electron injection layers in light-emitting devices, we prepared blue fluorescent OLEDs. Therefore, a 40 nm thick PEDOT:PSS layer was spin-coated on top of ITO covered glass substrates. Then, a 70 nm thick layer of the light-emitting polymer (SPB-02T) was spin-coated followed by an electron injection layer. As electron injection layer, spin-coated films of PEI and PEIE were used and their performances were compared to evaporated films of calcium. Finally, 100 nm of silver was evaporated as cathode material.

In Figure 4, the OLED stack and the luminance–current–voltage (LIV) characteristics, turn-on voltage (V_{ON}) and luminous efficiency of the fabricated OLEDs are shown. OLEDs using PEI(E) in combination with silver as cathode material exhibit comparable luminance levels to reference devices using Ca as cathode layer (Figure 4a, b). However, the performance of PEI(E)-OLEDs depends on the nominal polymer thickness. The nominal thickness of the PEI(E) layers on top of the organic emitter was estimated with the help of Figure 1c

OLEDs using a PEI layer with a nominal thickness of 2.7 nm showed the best performance of all OLEDs prepared in this work and exhibited a maximum luminance of almost 8000 cd m^{-2} at 8 V. By decreasing the nominal PEI thickness to values below 2.7 nm, it is still possible to prepare efficient devices. However, the reproducibility of these OLEDs is rather low. Increasing the nominal PEI thickness from 2.7 to 7.3 nm, leads to a decrease in both the current density and luminance by a factor of ~2 over the whole voltage range. By further increasing the nominal PEI thickness to 11.0 nm, both the current density and luminance decrease by another factor of about 4. This

dx.doi.org/10.1021/am500287y | ACS Appl. Mater. Interfaces 2014, 6, 6616–6622

thickness dependency of OLED performance can be ascribed to the insulating nature of PEI. A higher PEI thickness limits the current density and luminance of the OLEDs.

When comparing the LIV characteristics of PEI- and Ca-OLEDs, a qualitatively different behavior is obvious. Reference devices using Ca as cathode layer show higher luminance values at voltages below 4.5 V and thus exhibit lower turn-on voltages. At voltage levels above 4.5 V the situation changes and PEI-OLEDs start to outperform reference devices. At 8 V the maximum luminance of PEI-OLEDs is around 8000 cd m^{-2}, which is almost four times the maximum value observed for reference OLEDs. The reason for this behavior is probably related to the different nature of the cathode/semiconductor contact. For Ca, an almost ohmic contact can be expected, whereas in the case of PEI, a tunneling contact between Ag and the semiconductor should be formed.

Figure 4b shows the LIV characteristics of OLEDs using PEIE as electron injection layers. Particularly for voltages below 6 V, a thickness dependency of OLED performance is also observed for these OLEDs. OLEDs using PEIE with a nominal thickness of 3.7 nm exhibit the best performance. Increasing the nominal polymer thickness, leads to an increase in V_{ON}. For voltages above 6.5 V, however, all three PEIE concentrations deliver nearly the same luminance values. At 8 V, PEIE-OLEDs show a luminance of about 3000 cd m^{-2}, which is 50% more than the maximum luminance of our reference OLEDs.

In Figure 4d, the maximum luminous efficiencies of the prepared OLEDs, averaged over at least 4 different devices, are plotted against the respective nominal thicknesses of the PEI(E) layers. Starting from a pure silver cathode, the luminous efficiency rises from 0.06 to ~3 cd A^{-1}, when the nominal PEI thickness is increased to ~1 nm. This is 33% more than the maximum luminous efficiency measured for our reference OLEDs, which is ~2.25 cd A^{-1}. Further increasing the PEI thickness up to 11.5 nm moderately lowers the observed luminous efficiency to ~1.8 cd A^{-1}. This effect can again be explained by the insulating nature of the PEI layer.

In the case of PEIE, a similar behavior was observed. Increasing the nominal thickness up to 4 nm leads to a rise in luminous efficiency to a value of ~2.2 cd A^{-1}, which equals the efficiency of our reference devices. However, luminous efficiencies saturate at this point and increasing the PEIE thickness up to 11 nm has no influence anymore. This behavior can be correlated to the Ag/PEIE work functions presented in Figure 2. Starting from a pure silver sample, the measured Ag/PEIE work functions first decrease with increasing nominal polymer thickness and eventually saturate at thicknesses of more than 4 nm.

In Figure 4e, V_{ON} of the prepared OLEDs is plotted against the thickness of the PEI(E) layers. Here, V_{ON} is defined as the voltage at which a luminance of 1 cd m^{-2} is achieved. OLEDs using pure silver as cathode layer exhibit a turn-on voltage of ~8 V. Using a 0.3 nm thick PEI layer in addition to silver leads to a decrease of V_{ON} to 4.2 V. By increasing the nominal PEI thickness to 1 nm, V_{ON} can be further reduced to a minimum value of 3.8 V. This decrease of the measured turn-on voltages with increasing nominal PEI thickness can be attributed to an increasing polymer coverage and thus a decreasing cathode work function. However, the situation changes for layers with a nominal thickness of more than 1 nm. Then, V_{ON} rises with increasing nominal thickness until eventually a V_{ON} of 5.5 V is observed for samples with an 11 nm thick PEI layer. This thickness dependent increase in V_{ON} can be ascribed to the insulating nature of thicker PEI films.

In the case of PEIE, the qualitative behavior is very similar. Increasing the nominal thickness up to 4 nm leads to a decrease in V_{ON} to a minimal value of 4.3 V. For larger nominal PEIE thicknesses, V_{ON} rises and a turn-on voltage of about 4.7 V is observed at ~12 nm. These results can be understood in context of the cathode work functions presented in Figure 2. It was observed that the Ag/PEIE work function first decreases with increasing nominal PEIE thickness and eventually saturates. As the saturation regime starts at a thickness of ~4 nm, the lowest turn-on voltage is expected at this point. Larger PEIE thicknesses have no positive influence on the cathode work function anymore but just enlarge the thickness of the insulating polymer layer. This leads to the observed rise in V_{ON}. Reference OLEDs exhibit the lowest turn-on voltages of all OLEDs measured in this work with values of about 3.2 V. This is attributed to the low work function of Ca which is <3 eV.

Shelf Lifetime of PEI(E) OLEDs. Since aqueous solutions of PEI and PEIE are stable in air for more than a year,[21] OLEDs using these polymers instead of Ca as electron injection layer should exhibit strongly improved shelf lifetimes. In order to examine this, OLEDs with Ca, 3.4 nm PEI and 3.8 nm PEIE, respectively, were solution prepared, encapsulated and stored in ambient conditions for up to 4 weeks. Figure 5 shows photographs of the fabricated OLEDs under operation when they were freshly prepared, 2 weeks and 4 weeks after preparation. Right after preparation, the light emission of all three OLEDs is very homogeneous. Slight differences in color are due to the auto white balance and exposure settings of the camera that was used for taking the pictures.

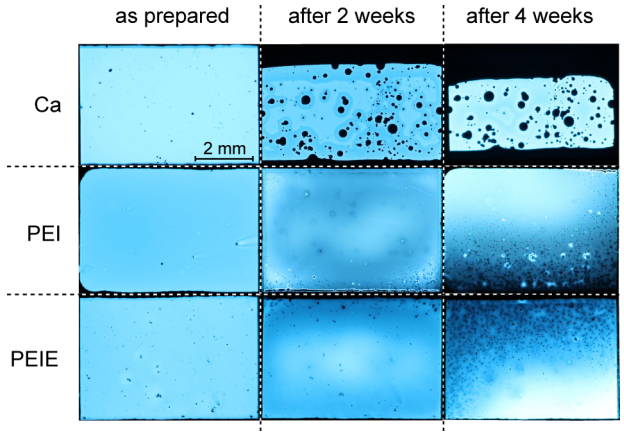

Figure 5. Photographs of OLED pixels, using different electron injection layers, under operation. Before pictures were taken, OLEDs had been stored in ambient atmosphere for different amounts of time. PEI- and PEIE-OLEDs exhibit almost no dark spots 2 weeks after preparation.

In the case of Ca-OLEDs, there are dark spots visible 2 weeks after preparation. Furthermore, the emission area is reduced from the edge of the device. Altogether, these defects account for 27% of the pixel's total area. Both types of defects are probably due to calcium being oxidized by water residues from the PEDOT:PSS layer and oxygen which diffuses through the adhesive of the encapsulation foil (topmost part). In case of the PEI- and PEIE-OLEDs, there are considerably less defects visible. Dark spots are hardly present and the size of the light-emitting area equals 97% and 99.5% of its original size for PEI

dx.doi.org/10.1021/am500287y | ACS Appl. Mater. Interfaces 2014, 6, 6616−6622

and PEIE, respectively. However, the light emission is not as homogeneous as on the first photographs. This could arise from a degradation of either PEI(E) or the light-emitting polymer.

Four weeks after preparation, the area of the Ca-OLED that is still emitting light decreased to 53% of its original size. PEI- and PEIE-OLEDs are also considerably degraded 4 weeks after preparation. The pixels show dark spots and the emission areas of the OLEDs are reduced from the edge of the encapsulation foil (bottom part for PEI-OLED and top part for PEIE-OLED). This indicates that PEI and PEIE are degraded by oxygen that diffuses through the adhesive of the encapsulation foil. The size of the light-emitting area of these OLEDs equals 76 and 92% of its original size for PEI and PEIE, respectively. These results confirm that the shelf lifetime of OLEDs can be enhanced by the use of polymeric electron injection layers.

CONCLUSION

PEI and PEIE were used as electron injection layers in solution-processed OLEDs in combination with Ag as stable cathode. The performance of the OLEDs was correlated to the nominal thickness of the PEI(E) layers and the induced work-function shift of the silver electrode. Therefore, PEI and PEIE were spin-coated on top of silver substrates and the resulting films were characterized by photoelectron spectroscopy. XPS was used to estimate the nominal thickness of the polymer layers and values between 1.7 and 12.2 nm were found. UPS measurements confirmed that these layers reduced the work function of the underlying silver layer. A strong thickness dependency of the resulting work function was observed for nominal polymer thicknesses below 5 nm. Above 5 nm, the measured work functions started to saturate and were thickness independent at higher thicknesses. Maximum work-function shifts were $\Delta\Phi$ = 1.5 eV for PEI and $\Delta\Phi$ = 1.3 eV for PEIE. AFM images revealed that the two observed work-function regimes can be explained by the coverage of the samples. For small nominal thicknesses, PEI and PEIE form islands and cover the underlying silver substrates only partially. These island grow in size as the nominal thickness is increased, and an almost homogeneous PEI(E) layer is present at nominal thicknesses of more than 10 nm. Furthermore, we spin-coated blue fluorescent OLEDs using PEI(E) with various nominal thicknesses as electron injection layer. In the case of PEI, an optimal polymer thickness between 1 and 4 nm was determined, whereas for PEIE, OLEDs with polymer thicknesses between 4 and 12 nm performed comparable. OLEDs using PEI as electron injection layer exhibited a luminous efficiency and maximum luminance of up to 3.0 cd A^{-1} and ~8000 cd m^{-2} and hence outperformed our Ca reference OLEDs. PEIE-OLEDs performed comparable to our reference devices with luminous efficiencies of ~2.2 cd A^{-1} and a maximum luminance of almost 3000 cd m^{-2}. Finally, we observed that OLEDs using PEI and PEIE as electron injection layer exhibit improved shelf lifetimes compared to reference devices using Ca.

EXPERIMENTAL SECTION

Sample Preparation. PEI and PEIE solutions were prepared by dissolving the polymers in 2-methoxyethanol. Ag/PEI(E) samples were prepared as follows: glass substrates were subsequently cleaned in Acetone and Isopropanol under sonification for 15 min, respectively. Afterward, 100 nm of silver was evaporated in an vacuum system with a base pressure of 2×10^{-7} mbar. PEI and PEIE solutions were spin-coated in a glovebox directly connected to the evaporation chamber, so that the samples did not get in contact with air. Spin-coating parameters were ω = 5000 rpm, a = 1000 rpm/s, and t = 60 s. After spin-coating, the samples were annealed on a hot plate at 120 °C for 10 min.

OLEDs were prepared as follows: glass substrates covered by 140 nm of ITO were subsequently cleaned in Acetone and Isopropanol under sonication for 15 min, respectively, and treated by O_2 plasma for 5 min. Afterward, PEDOT:PSS solution, acquired from Heraeus, was filtered with a 0.45 μm PVDF filter, spin-coated in ambient conditions and annealed on a hot plate at 130 °C for 15 min. Spin-coating parameters were ω = 2500 rpm, a = 1000 rpm/s and t = 30 s so that a layer of about 40 nm was obtained. SPB-02T (light emitting polymer), acquired from Merck KGaA, was dissolved in Mesitylene with a concentration of 10 g/L and spin-coated in ambient conditions. Spin-coating parameters were ω = 1800 rpm, a = 1000 rpm/s and t = 30 s and delivered a layer thickness of approximately 70 nm. Afterward, the samples were annealed on a hot plate located inside a glovebox at 120 °C for 30 min. In case of the reference OLEDs, 10 nm of Ca followed by 100 nm of Ag were evaporated as cathode layer in a vacuum system with a base pressure of 1×10^{-7} mbar. In case of the OLEDs using PEI(E) as electron injection layer, PEI(E) was spin-coated under a nitrogen atmosphere with ω = 5000 rpm, a = 1000 rpm/s, and t = 60 s. Afterward, the samples were annealed in a vacuum oven at 120 °C for 15 min. Finally, 100 nm of silver were evaporated as cathode. All OLEDs were encapsulated by barrier foil, acquired from 3M.

Photoelectron Spectroscopy Measurements. The photoelectron spectroscopy characterization was performed using a PHI VersaProbe II scanning XPS microprobe located at the InnovationLab in Heidelberg. The spectrometer is equipped with a monochromatized Al–K_α X-ray source, an Omicron HIS 13 helium discharge lamp, and a concentric hemispherical analyzer. Detail spectra of the core level lines were recorded with a pass energy of 11.75 eV, for the secondary electron edges 0.58 eV were chosen. The spectra and secondary electron edges are referenced in binding energy with respect to the Fermi edge and the core level lines of in situ cleaned Au, Ag, and Cu metal foils.

Atomic Force Microscopy Images. AFM images were recorded with a DME DS 95 Dualscope AFM in ambient conditions. We measured in AFM tapping mode using highly doped silicon cantilevers from NanoWorld (Arrow NCR). These cantilevers have resonance frequencies of about 285 kHz and tip radii of less than 10 nm.

ASSOCIATED CONTENT

Supporting Information

UPS secondary electron edge spectra as well as XPS C 1s and N 1s core level spectra of Ag/PEI(E) samples are available as Supporting Information. This material is available free of charge via the Internet at http://pubs.acs.org.

AUTHOR INFORMATION

Corresponding Author

*Sebastian Stolz, Email: Sebastian.stolz@kit.edu.

Notes

The authors declare no competing financial interest.

ACKNOWLEDGMENTS

The authors are thankful to I. Ringle for experimental support and fruitful discussion. We acknowledge financial support via the projects NanoPEP (FKZ 13N12127) and MORPHEUS (FKZ 13N11705) of the Leading-Edge Cluster Forum Organic Electronics managed by InnovationLab GmbH within the High-Tech Strategy for Germany of the Federal Ministry of Education and Research. We furthermore acknowledge the German Federal Ministry of Education and Research for

financial support via the project MESOMERIE (FKZ 13N10721).

REFERENCES

(1) Burrows, P. E.; Bulovic, V.; Forrest, S. R.; Sapochak, L. S.; McCarty, D. M.; Thompson, M. E. Reliability and Degradation of Organic Light Emitting Devices. *Appl. Phys. Lett.* **1994**, *65*, 2922−2924.

(2) Berntsen, A. J. M.; van de Weijer, P.; Croonen, Y.; Liedenbaum, C. T. H. F.; Vleggaar, J. J. M. Stability of Polymer Light-Emitting Diodes. *Philips J. Res.* **1998**, *51*, 511−525.

(3) Sheats, J. R.; Roitman, D. B. Failure Modes in Polymer-Based Light-Emitting Diodes. *Synth. Met.* **1998**, *95*, 79−85.

(4) Lim, S. F.; Wang, W.; Chua, S. J. Degradation of Organic Light-Emitting Devices due to Formation and Growth of Dark Spots. *Mater. Sci. Eng., B* **2001**, *85*, 154−159.

(5) Lim, F.; Wang, W.; Chua, S. J. Understanding Dark Spot Formation and Growth in Organic Light- Emitting Devices by Controlling Pinhole Size and Shape **. *Adv. Funct. Mater.* **2002**, *12*, 513−518.

(6) Choong, V.; Park, Y.; Gao, Y.; Wehrmeister, T.; Müllen, K.; Hsieh, B. R.; Tang, C. W. Dramatic Photoluminescence Quenching of Phenylene Vinylene Oligomer Thin Films Upon Submonolayer Ca Deposition. *Appl. Phys. Lett.* **1996**, *69*, 1492−1494.

(7) Park, Y.; Choong, V.; Hsieh, B. R.; Tang, C. W.; Gao, Y. Gap-State Induced Photoluminescence Quenching of Phenylene Vinylene Oligomer and its Recovery by Oxidation. *Phys. Rev. Lett.* **1997**, *78*, 3955−3958.

(8) Choong, V.; Park, Y.; Shivaparan, N.; Tang, C. W.; Gao, Y. Deposition-Induced Photoluminescence Quenching of Tris-(8-hydroxyquinoline) aluminum. *Appl. Phys. Lett.* **1997**, *71*, 1005−1007.

(9) Stoessel, M.; Wittmann, G.; Staudigel, J.; Steuber, F.; Blässing, J.; Roth, W.; Klausmann, H.; Rogler, W.; Simmerer, J.; Winnacker, A.; Inbasekaran, M.; Woo, E. P. Cathode-Induced Luminescence Quenching in Polyfluorenes. *J. Appl. Phys.* **2000**, *87*, 4467−4475.

(10) Huang, J.; Xu, Z.; Yang, Y. Low-Work-Function Surface Formed by Solution-Processed and Thermally Deposited Nanoscale Layers of Cesium Carbonate. *Adv. Funct. Mater.* **2007**, *17*, 1966−1973.

(11) Hsiao, C.-C.; Hsiao, A.-E.; Chen, S.-A. Design of Hole Blocking Layer with Electron Transport Channels for High Performance Polymer Light-Emitting Diodes. *Adv. Mater.* **2008**, *20*, 1982−1988.

(12) Wetzelaer, G. A. H.; Najafi, A.; Kist, R. J. P.; Kuik, M.; Blom, P. W. M. Efficient Electron Injection from Solution-Processed Cesium Stearate Interlayers in Organic Light-Emitting Diodes. *Appl. Phys. Lett.* **2013**, *102*, 053301−1−053301−4.

(13) Wang, G.; Jiu, T.; Sun, C.; Li, J.; Li, P.; Lu, F.; Fang, J. Highly Efficient Organic Photovoltaics via Incorporation of Solution-Processed Cesium Stearate as the Cathode Interfacial Layer. *ACS Appl. Mater. Interfaces* **2014**, *6*, 833−838.

(14) Hoven, C. V.; Garcia, A.; Bazan, G. C.; Nguyen, T. Recent Applications of Conjugated Polyelectrolytes in Optoelectronic Devices. *Adv. Mater.* **2008**, *20*, 3793−3810.

(15) Guan, X.; Zhang, K.; Huang, F.; Bazan, G. C.; Cao, Y. Amino N-Oxide Functionalized Conjugated Polymers and their Amino-Functionalized Precursors: New Cathode Interlayers for High-Performance Optoelectronic Devices. *Adv. Funct. Mater.* **2012**, *22*, 2846−2854.

(16) Wu, H.; Huang, F.; Mo, Y.; Yang, W.; Wang, D.; Peng, J.; Cao, Y. Efficient Electron Injection from a Bilayer Cathode Consisting of Aluminum and Alcohol-/Water-Soluble Conjugated Polymers. *Adv. Mater.* **2004**, *16*, 1826−1830.

(17) Huang, F.; Wu, H.; Cao, Y. Water/Alcohol Soluble Conjugated Polymers as Highly Efficient Electron Transporting/Injection Layer in Optoelectronic Devices. *Chem. Soc. Rev.* **2010**, *39*, 2500−2521.

(18) Zeng, W.; Wu, H.; Zhang, C.; Huang, F.; Peng, J.; Yang, W.; Cao, Y. Polymer Light-Emitting Diodes with Cathodes Printed from Conducting Ag Paste. *Adv. Mater.* **2007**, *19*, 810−814.

(19) Zheng, H.; Zheng, Y.; Liu, N.; Ai, N.; Wang, Q.; Wu, S.; Zhou J.; Hu, D.; Yu, S.; Han, S.; Xu, W.; Luo, C.; Meng, Y.; Jiang, Z.; Chen, Y.; Li, D.; Huang, F.; Wang, J.; Peng, J.; Cao, Y. All-Solution Processed Polymer Light-Emitting Diode Displays. *Nat. Commun.* **2013**, *4*. doi:10.1038/ncomms2971.

(20) Fan, Q.-L.; Lu, S.; Lai, Y.-H.; Hou, X.-Y.; Huang, W. Synthesis, Characterization, and Fluorescence Quenching of Novel Cationic Phenyl-Substituted Poly (p-phenylenevinylene)s. *Macromolecules* **2003**, *36*, 6976−6984.

(21) Zhou, Y.; Fuentes-Hernandez, C.; Shim, J.; Meyer, J.; Giordano, A. J.; Li, H.; Winget, P.; Papadopoulos, T.; Cheun, H.; Kim, J.; Fenoll, M.; Dindar, A.; Haske, W.; Najafabadi, E.; Khan, T. M.; Sojoudi, H.; Barlow, S.; Graham, S.; Brédas, J.-L.; Marder, S. R.; Khan, A.; Kippelen, B. A Universal Method to Produce Low-Work Function Electrodes for Organic Electronics. *Science* **2012**, *336*, 327−332.

(22) Kyaw, A. K. K.; Wang, D. H.; Gupta, V.; Zhang, J.; Chand, S.; Bazan, G. C.; Heeger, A. J. Efficient Solution-Processed Small-Molecule Solar Cells with Inverted Structure. *Adv. Mater.* **2013**, *25*, 2397−2402.

(23) Saracco, E.; Bouthinon, B.; Verilhac, J.-M.; Celle, C.; Chevalier, N.; Mariolle, D.; Dhez, O.; Simonato, J.-P. Work Function Tuning for High-Performance Solution-Processed Organic Photodetectors with Inverted Structure. *Adv. Mater.* **2013**, *25*, 6534−6538.

(24) Xiong, T.; Wang, F.; Qiao, X.; Ma, D. A Soluble Nonionic Surfactant as Electron Injection Material for High-Efficiency Inverted Bottom-Emission Organic Light Emitting Diodes. *Appl. Phys. Lett.* **2008**, *93*, 123310−1−123310−3.

(25) Kim, Y.-H.; Han, T.-H.; Cho, H.; Min, S.-Y.; Lee, C.-L.; Lee, T.-W. Polyethylene Imine as an Ideal Interlayer for Highly Efficient Inverted Polymer Light-Emitting Diodes. *Adv. Funct. Mater.* **2014**, DOI: 10.1002/adfm.201304163.

(26) Udum, Y.; Denk, P.; Adam, G.; Apaydin, D. H.; Nevosad, A.; Teichert, C.; White, M. S.; Sariciftci, N. S.; Scharber, M. C. Inverted Bulk-Heterojunction Solar Cell With Cross-Linked Hole-Blocking Layer. *Org. Electron.* **2014**, DOI: 10.1016/j.orgel.2014.02.009.

(27) Kim, D.; Jeong, S.; Moon, J.; Kang, K. Ink-Jet Printing of Silver Conductive Tracks on Flexible Substrates. *Mol. Cryst. Liq. Cryst.* **2006**, *459*, 45/[325]−55/[335].

(28) Jeong, J.-A.; Kim, J.; Kim, H.-K. Ag Grid/ITO Hybrid Transparent Electrodes Prepared by Inkjet Printing. *Sol. Energy Mater. Sol. Cells* **2011**, *95*, 1974−1978.

(29) Hilali, M. M.; Nakayashiki, K.; Khadilkar, C.; Reedy, R. C.; Rohatgi, A.; Shaikh, A.; Kim, S.; Sridharan, S. Effect of Ag Particle Size in Thick-Film Ag Paste on the Electrical and Physical Properties of Screen Printed Contacts and Silicon Solar Cells. *J. Electrochem. Soc.* **2006**, *153*, A5−A11.

(30) Duraisamy, N.; Ponniah, G.; Jo, J.; Choi, K.-H. Structural and Electrical Properties of Ag Grid/Poly(3,4-ethylenedioxythiophene):Poly(styrenesulfonate) Coatings for Diode Application Through Advanced Printing Technology. *J. Nanosci. Nanotechnol.* **2013**, *13*, 5957−5963.

(31) Klein, A.; Mayer, T.; Thissen, A.; Jaegermann, W. Photoelectron Spectroscopy in Materials Science and Physical Chemistry. *Bunsen-Mag.* **2008**, *4*, 124−139.

(32) Gries, W. H. A. Universal Predictive Equation for the Inelastic Mean Free Pathlengths of X-ray Photoelectrons and Auger Electrons. *Surf. Interface Anal.* **1996**, *24*, 38−50.

(33) Kang, H.; Hong, S.; Lee, J.; Lee, K. Electrostatically Self-Assembled Nonconjugated Polyelectrolytes as an Ideal Interfacial Layer for Inverted Polymer Solar Cells. *Adv. Mater.* **2012**, *24*, 3005−3009.